Proceedings of the 28th IEEE
EMBS Annual International Conference
New York City, USA, Aug 30-Sept 3, 2006

Knowledge-driven 3-D Extraction of the Masseter from MR Data

H.P. Ng[1, 2], S.H. Ong[3], K.W.C. Foong[1, 4], P.S. Goh[5], W.L. Nowinski[2]

[1]NUS Graduate School for Integrative Sciences and Engineering, Singapore
[2]Biomedical Imaging Lab, Agency for Science Technology and Research, Singapore
[3]Department of Electrical and Computer Engineering, National University of Singapore
[4]Department of Preventive Dentistry, National University of Singapore
[5]Department of Diagnostic Radiology, National University of Singapore

Abstract- In this paper, we propose a knowledge-driven highly automatic methodology for extracting the masseter from magnetic resonance (MR) data sets for clinical purposes. The masseter is a muscle of mastication which acts to raise the jaw and clench the teeth. In our initial work, we designed a process which allowed us to perform 2-D segmentation of the masseter on 2-D MR images. In the methodology proposed here, we make use of ground truth to first determine the index of the MR slice in which we will carry out 2-D segmentation of the masseter. Having obtained the 2-D segmentation, we will make use of it to determine the region of interest (ROI) of the masseter in the other MR slices belonging to the same data set. The upper and lower thresholds applied to these MR slices, for extraction of the masseter, are determined through the histogram of the 2-D segmented masseter. Visualization of the 3-D masseter is achieved via volume rendering. Our methodology has been applied to five MR data sets. Validation was done by comparing the segmentation results obtained by using our proposed methodology against manual contour tracings, obtaining an average accuracy of 83.5%

1. INTRODUCTION

Maxillofacial surgeries are carried out to correct discrepancies in spatial relationship between the upper and lower jaws, and in the process, improve the individual's facial appearance and the ability to chew, and perhaps a higher sense of self-confidence and quality of life, respectively. The facial bones of interest are the mandible (lower jaw) and maxilla (upper jaw). The facial muscles of interest are the muscles of mastication, which include the masseter, lateral pterygoid, medial pterygoid and temporalis. We focus on the masseter here.

Pre-surgical facial models are created to aid clinicians in their surgical planning. Koch et al. constructed a 3D physics-based facial model from CT and laser range scans [1]. 3D volumetric elasticity is applied in the construction of the model to allow the representation of important volumetric effects such as incompressibility in a natural and physically accurate manner. Another recent physically based facial model used for pre-surgery simulation was developed by Gladilin et al. and used for static soft tissue prediction and muscle simulation [2]. This model uses the linear elastic modeling approach to simplify the highly complicated biomechanical behavior of different tissue types. In this model, it has been assumed that different tissue groups have similar properties. These models and the one in [3] do not provide clinicians with an idea on the exact location, shape and size of the different muscles of mastication.

In the actual surgical procedure, surgeons first detach the relevant muscles of mastication from the surface of the jaw bones, make adjustments to the jaws and then re-attach the muscles of mastication back to the jaws. During surgical planning for maxillofacial surgeries, surgeons have to decide the adjustments or displacements to be made to the upper jaw (maxilla) or the lower jaw (mandible). As the jaws are shifted, the muscles of mastication will correspondingly change in location, shape and size. Knowledge of the location, shape and size of the facial muscles, before and after surgery, will increase the chances of a successful facial surgery.

There is an increasing emphasis on 3-D medical image segmentation, and many established techniques such as the level set approach [4] and graph cuts [5] have been used for 3-D image segmentation. However, their computational load may be high. To reduce computational complexity, some proposed methodologies apply 2-D techniques sequentially to the slices of a 3-D image [6], [7]. The complexity of how the targeted objects have been defined is another factor considered before deciding on the technique used.

Our methodology is designed for extraction of the masseter, which is a complex structure without clear boundaries at times, from MR data sets. The methodology is a 3-stage process. In the first stage, we make use of ground truth to first determine the index of the MR slice in which we will carry out 2-D segmentation of the masseter. We call this the reference image. In the second stage, we apply the technique which we developed in our initial work [8] to segment the masseter. In the third stage, through the 2-D segmentation, we specify the ROI for the other slices in the MR data set. The upper and lower thresholds are also determined via the 2-D segmentation of the masseter.

The paper first describes the proposed methodology in Section 3. Results and discussion are provided in Section 4. We conclude the paper in Section 5.

2. MATERIALS

The MR data were obtained by a 1.5 Tesla MR unit. The MR imaging protocol used is the T1 fast low angle shot (FLASH) with the parameters (1mm thickness, 512x512

matrix, 240 mm FOV, TR = 9.93, TE = 4.86). Ten MR data sets were collected. A slice of MR image with the masseter marked out is in Fig.1.

Fig.1: MR image with masseter marked out

3. Methodology

The proposed methodology is a 3-stage process, as illustrated in Figure 2.

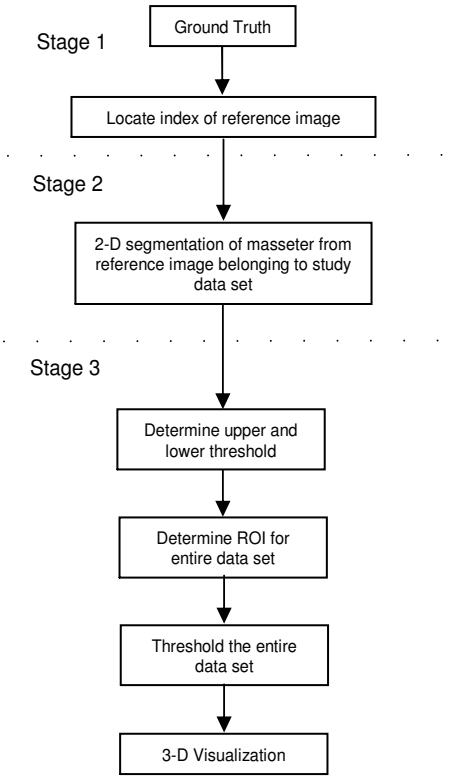

Fig. 2: Flowchart of methodology

A. Location of reference image in MR data set

We have five MR data sets where the masseter has been manually segmented from all the image slices. They serve as the ground truth. In the first stage, we make use of the ground truth to determine the index of the reference image. From each set of ground truths, we input the index of the image where the masseter first starts to appear (Fig. 3a) and the index of the image where the masseter last appears (Fig. 3b). We compute the surface area of the masseter (in terms of number of pixels) for all the slices of MR images, from the starting slice to the ending slice. After this, we computed the percentile where the image with the largest surface area of the masseter is located. This is the reference image.

From the five sets of ground truth, we tabulate the results in Table 1 and deduce that the reference image exists at the 48.7th percentile between the starting index and ending index.

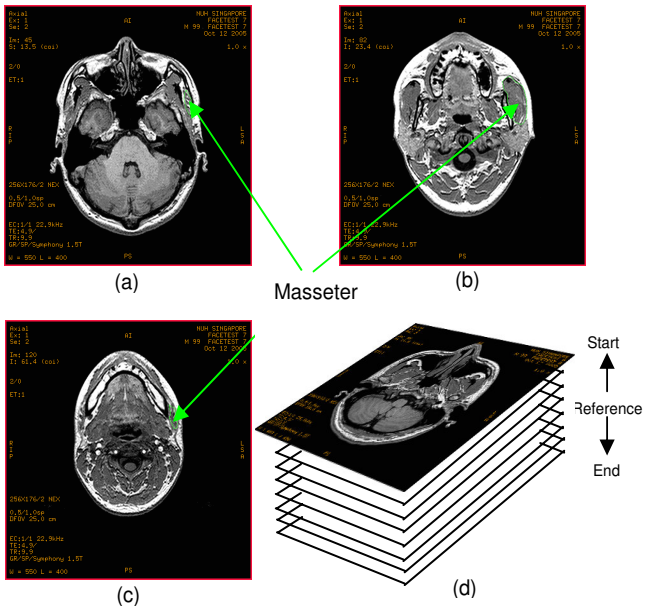

Fig. 3: (a) Image where masseter first appear; (b) Image where masseter appear largest; (c) Image where masseter last appear; (d) Stack of MR images

Table 1: Location of reference image

(percentile={[(RI-SI)+1]/[EI-SI]}x100%)

Ground Truth Data Set	Start Index (SI)	End Index (EI)	Reference Index (RI)	Percentile
1	51	115	81	47.69%
2	41	108	73	48.53%
3	45	120	81	48.68%
4	46	122	83	49.35%
5	41	113	76	49.32%
			Mean	**48.71%**

B. 2-D segmentation of masseter

After determining the percentile which the reference image belongs to, we make use of the 2-D segmentation methodology, which we proposed in [8], to segment the masseter from the reference image belonging to the study data set. The inputs to the 2-D segmentation methodology are the five reference images belonging to the five sets of ground truth and a reference image from the study data set. The output is the 2-D segment of the masseter from the reference image belonging to the study data set.

Through the five reference images from the ground truth, a spatial relationship between the masseter ROI and head ROI is developed. Based on this relationship, the system is then able to identify the masseter ROI in the study image. After identifying the ROI, we make use of a template of the masseter, which is obtained via manual contour tracings, to

obtain an initial segmentation of the facial muscle. This initial segmentation serves as the initialization to the gradient vector flow (GVF) snake to obtain the final segmentation result. A sample of the automatically detected ROI and segmentation result are shown in Figs. 4a and 4b, respectively.

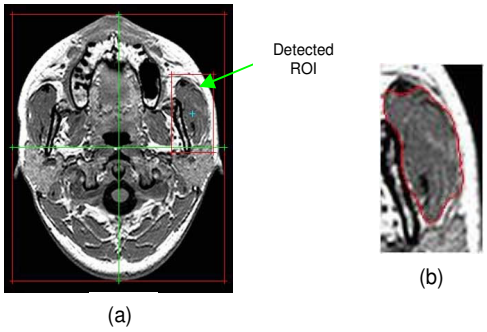

Fig. 4: (a) Detected masseter ROI; (b) Segmented masseter

C. Thresholding of study data set and 3-D visualization

The 2-D segmentation of the masseter from the reference image of the study data set is used to specify the constraints, for the remaining image slices between the starting and ending indices.

We first make use of the histogram of the 2-D segmented masseter to determine the upper (T_{high}) and lower (T_{low}) thresholds. A sample histogram and its corresponding cumulative histogram are in Figs. 5a and 5b, respectively. It can be observed from Fig. 5a that outliers are present. We set the lower and upper thresholds at the 5th and 95th percentile of the cumulative histogram respectively. The threshold values are 52 and 168 for this example. The justification of threshold values will be investigated in future work.

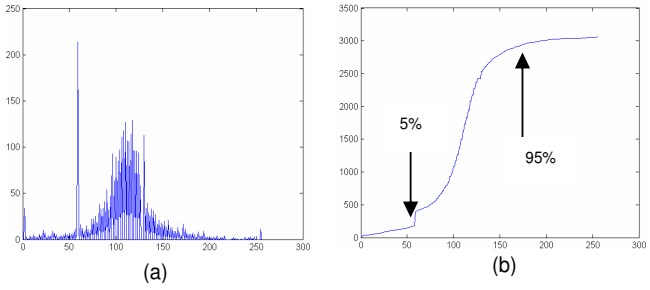

Fig. 5: (a) Histogram of segmented masseter (b) Corresponding cumulative histogram

The masseter ROI for the image slices between starting and ending index is also determined through the 2-D segmentation of the masseter. We first define a rectangular ROI, known as reference ROI and shown in red in Fig. 6, which bounds the segmented masseter in reference image. To ensure that it bounds the masseter entirely, we define the ROI for other slices as the reference ROI scaled by a factor *s*. Here we set *s* to be 1.3. The newly defined ROI is shown in Fig. 6.

With the ROI defined, we can threshold the images between the starting and ending index, using T_{upper} and T_{lower} derived earlier on. After thresholding, muscle and soft tissue, which has similar gray level as the muscles, remain. Hence, we need to differentiate the muscle from the unwanted soft tissue.

The reference image has the largest surface area of the masseter and as the image index increases or decreases, the surface area will gradually decrease. Hence, we implement a masking step in our algorithm. In the ROI, pixels within the mask remain else they are removed. The mask is defined as:

$(Mask)_{k-1}$= Segmentation from $(Image)_k$, k < reference index
$(Mask)_{k+1}$= Segmentation from $(Image)_k$, k > reference index

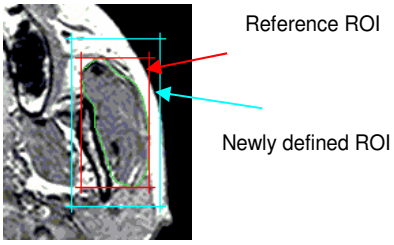

Fig. 6: Definition of masseter ROI

After thresholding and mask-correlation, we use morphological closing to fill up the holes in the masseter. Volume rendering [6] is utilized to visualize the 3-D masseter. It directly displays a sampled 3D scalar field without first fitting geometric primitives to the sample.

4. RESULTS AND DISCUSSION

The proposed methodology was applied to five study data sets. Some 3-D visualizations, together with a 3-D histogram of a masseter are shown in Fig.7 and Fig. 8 respectively.

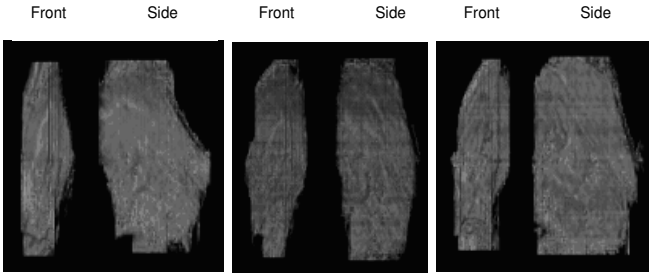

Fig. 7: 3-D visualizations of the masseter

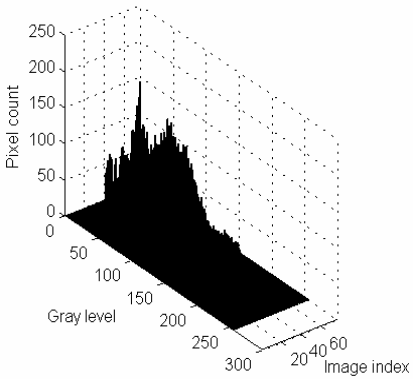

Fig. 8: 3-D histogram of masseter

Numerical verifications are carried out on a per-slice basis. The accuracy index:

$$\mathrm{AI} = 2 \times \left(\frac{N(M_{area} \cap S_{area})}{N(M_{area}) + N(S_{area})} \right)$$

is used, where M_{area} and S_{area} are the areas belonging to the manual segmentations and our segmentation results, respectively. $N(M_{area})$ refers to the number of pixels in M_{area}. The average accuracy achieved is 83.5%. Fig. 9 shows an AI against image index plot for one of the study data sets. It can be observed that as the image index decreases towards the starting index or increases towards the ending index, AI will decrease. This is because at these regions, the probability of the masseter not having clear distinct boundaries increases.

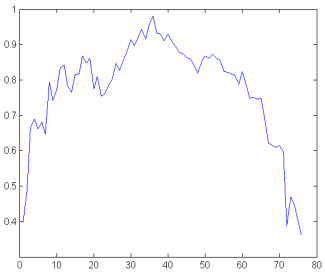

Fig. 9: AI vs. Image index

In the area of 3-D image segmentation, there are several established techniques. The level set approach and graph cuts are good examples. However, their computational load may be high. The methodology proposed here is more direct as compared to them. However, we will be looking forward to improving the accuracy. Relating the masseter to the skull, as illustrated in Fig. 10 is also part of our future work.

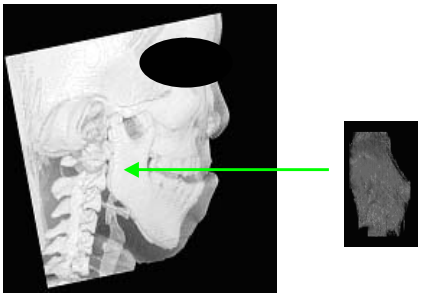

Fig. 10: Relating muscle to the skull

5. CONCLUSION

We have proposed a highly automatic methodology for extracting the masseter from MR images, which to our best knowledge, is currently unavailable. Our methodology involves the use of ground truth to first determine a reference image. 2-D segmentation of the masseter from the reference image is then carried out. We utilize this 2-D segmentation to lay down constraints (threshold values and ROI) which enable us to extract the masseter from the other slices in the data set. Volume rendering is used to visualize the 3-D masseter. Currently, the average accuracy achieved is 83.5% and we are looking forward to improving it.

ACKNOWLEDGMENTS

This project is funded by NUS R-222-000-011-112 from the Faculty of Dentistry, National University of Singapore. The first author is grateful to Agency for Science, Technology and Research (A*Star), Singapore for funding his PhD studies. The authors thank Mr Christopher Au, Principal Radiographer at National University Hospital, Singapore for rendering his assistance and expertise in data acquisition.

REFERENCES

[1] R. Koch, S. Roth, M. Gross, A. Zimmermann, H. Sailer, “A Framework for Facial Surgery Simulation”, Proceedings of 18th Spring Conference on Computer Graphics, pp. 33-42, 2002

[2] E. Gladilin, S. Zachow, P. Deuflhard, H.C. Hege, "Anatomy and physics-based facial animation for craniofacial surgery simulations", Medical & Biological Engineering & Computing, vol.42, pp 167-170, 2004

[3] K. Maki, N. Inou, A. Takanishi, A.J. Miller, “Computer-assisted simulations in orthodontic diagnosis and the application of a new cone beam X-ray computed tomography”, Journal of Orthodontics and Craniofacial Research, vol. 6, pp. 179-182, 2002

[4] R. Malladi, J.A. Sethian, B.C. Vermuri, “Shape modelling with front propagation: A level set approach” IEEE. Trans. Pattern Analysis and Machine Intelligence, vol.17, pp.158-174, 1995

[5] Y. Boykov, V. Kolmogorov, “Computing geodesics and minimal surfaces via graph cuts”, Int. Conf. on Computer Vision (ICCV), vol.1, pp.26-33, 2003

[6] D.L. Pham, J.L. Prince, A.P. Dagher, et al., “An automated technique for statistical characterization of brain tissues in magnetic resonance image”, Int. Journal Pattern Recognition Artificial Intelligence, vol.11, pp.1189-1211, 1997

[7] Y. Ge, J.M. Fitzpatrick, B.M. Dawant, et al., “Accurate localization of cortical convolutions in MR brain images”, IEEE. Trans. On Medical Imaging, vol.15, pp.418-428, 1996

[8] H.P. Ng, S.H. Ong, P.S. Goh, K.W.C. Foong, W.L. Nowinski, “Template-based automatic segmentation of masseter using prior knowledge”, IEEE Southwest Symposium on Image Analysis and Interpretation, pp. 208-212, 2006

[9] A.B. Jani, C.A. Pelizzari, G.T. Chen, J. Roeske, R.J. Hamilton, R.L. Macdonald, F. Bova, K.R. Hoffmann, P.A. Sweeney, “Volume rendering quantification algorithm for reconstruction of CT volume-rendered structures”, IEEE Trans. on Medical Imaging, vol.19(1), pp. 12-24, 2000